

Catalysis Science & Technology

Accepted Manuscript



This is an *Accepted Manuscript*, which has been through the Royal Society of Chemistry peer review process and has been accepted for publication.

Accepted Manuscripts are published online shortly after acceptance, before technical editing, formatting and proof reading. Using this free service, authors can make their results available to the community, in citable form, before we publish the edited article. We will replace this *Accepted Manuscript* with the edited and formatted *Advance Article* as soon as it is available.

You can find more information about *Accepted Manuscripts* in the [Information for Authors](#).

Please note that technical editing may introduce minor changes to the text and/or graphics, which may alter content. The journal's standard [Terms & Conditions](#) and the [Ethical guidelines](#) still apply. In no event shall the Royal Society of Chemistry be held responsible for any errors or omissions in this *Accepted Manuscript* or any consequences arising from the use of any information it contains.

Cite this: DOI: 10.1039/c0xx00000x

www.rsc.org/xxxxxx

ARTICLE TYPE

Effect of TiO₂ crystal structure on the catalytic performance of Co₃O₄/TiO₂ catalyst for low-temperature CO oxidation

Jie Li,^a Guanzhong Lu,^{*a,b} Guisheng Wu,^b Dongsen Mao,^b Yanglong Guo^a, Yanqin Wang^a and Yun Guo^a

Received (in XXX, XXX) Xth XXXXXXXXX 20XX, Accepted Xth XXXXXXXXX 20XX

DOI: 10.1039/b000000x

The Co₃O₄ catalysts supported on TiO₂ with different crystalline structures (anatase (A), rutile (R) and P25 (Degussa)) were prepared by a deposition-precipitation method, and characterized by nitrogen adsorption/desorption, XRD, HR-TEM, EPR, Raman spectroscopy, XPS and H₂-TPR techniques. The results show that Co₃O₄/TiO₂(A) exhibited the highest activity among three Co₃O₄/TiO₂ catalysts: CO can be completely oxidized to CO₂ at -43 °C. When rutile TiO₂ or P25 were used as the support, its catalytic activity was decreased obviously, because the TiO₂ crystal structure has an influence on the physicochemical and catalytic properties of the Co₃O₄ catalysts. The results show that the Co₃O₄/TiO₂(A) catalyst contains Ti³⁺ species, which is of unstable state and can affect the properties of Co₃O₄ by the interaction between the deposited Co₃O₄ and anatase TiO₂ support. The Co₃O₄/TiO₂(A) catalyst exhibits highly defective structure and good oxygen adsorption ability. The reducibility of Co₃O₄ is improved by anatase TiO₂ support, resulting in Co₃O₄/TiO₂(A) possessing the better redox property than other Co₃O₄/TiO₂ catalysts, which is an important factor for its high catalytic activity.

1. Introduction

Low-temperature oxidation of CO, as one of the most extensively studied reactions in the heterogeneous catalysis field, is becoming increasingly important in cleaning air and lowering automotive emissions^{1,2}. For the catalysts for CO oxidation, the precious metals (Pd, Pt and nano-Au) are well-known catalysts with high activity³⁻⁶, but the reaction temperature of CO complete conversion over precious metals (such as Pt) are still pretty high and their stabilities are poor. To overcome the high cost of precious metals, researchers try to design and develop the non-precious metal catalysts, such as the metal oxide catalysts. Among them, cobalt oxide (Co₃O₄) is thought to be a potential catalyst⁷⁻¹⁰, because of its high activity for CO oxidation even at below 0 °C^{11,12}. Hence, the Co₃O₄ catalysts for low-temperature CO oxidation are widely studied,^{10,13,14} including mix-valenced CoO_x,⁹ supported Co₃O₄,¹² noble metal (Au, Pt) supported on Co₃O₄,^{11,12} and Fe(or Ce)-doped Co₃O₄ catalyst,^{15,16} etc. These researches above for Co₃O₄ catalysts are mainly focused on the preparation of Co₃O₄ and foreign element doping; for supported Co₃O₄ catalysts, their catalytic activities need still to be improved and the effects of structure and physicochemical properties of support on the catalytic performance of Co₃O₄ are less studied. Titanium oxide (TiO₂) is extensively used in the solid catalysts, particularly as a catalyst support¹⁷⁻²⁰. When nano-metal particles supported on TiO₂, there are often a strong metal-support interaction (SMSI)²¹. TiO₂ possesses multi-crystalline structures, and is mainly classified into anatase, rutile and brookite phases, among which anatase and rutile TiO₂ are generally used as engineering materials more frequently than the brookite phase

TiO₂. As a photo-catalyst, TiO₂ crystalline phases can affect obviously on its photo-catalytic activity²²⁻²⁴. Palladium supported on anatase TiO₂ shows a higher activity than that on rutile TiO₂ for the selective hydrogenation of long chain alkadienes, due to the superior SMSI between Pd and anatase TiO₂²⁵. Nanba *et al.*²⁶ studied the catalytic decomposition of acrylonitrile over Ag supported on TiO₂ with different crystal phases, and found that Ag/TiO₂ containing anatase TiO₂ exhibited higher NH₃ and N₂ selectivity at low and high temperatures, whereas Ag/TiO₂ with only rutile phase exhibited medium N₂ and higher NO_x selectivity at low and high temperatures. This may be that different crystalline phases of TiO₂ support can affect the SMSI¹⁸, electronic density, oxidation state, crystal size²⁰ and metal dispersion²⁷ of the deposited metal components. These changes in deposited metals (or metal oxides) supported on TiO₂ with different crystalline phases can have a dramatic impact on catalytic performance.

Herein, we investigated mainly the effect of TiO₂ crystalline phases on the catalytic performance of Co₃O₄/TiO₂ for CO oxidation, to look for the approach of preparing a high effective Co₃O₄/TiO₂ catalyst. Three kinds of TiO₂ with different crystalline structures were utilized as the supports of Co₃O₄ catalyst. We have found that Co₃O₄ supported on anatase TiO₂ (Co₃O₄/TiO₂(A)) exhibits very excellent catalytic activity and CO is completely converted at -43 °C. On the basis of the physicochemical properties of Co₃O₄/TiO₂(A) obtained, the role of different crystalline phases of TiO₂ on promoting its catalytic activity was discussed.

2. Experimental Section

2.1. Catalysts preparation

The TiO₂ supports used here are anatase phase (TiO₂(A)), P25 and rutile phase (TiO₂(R)) respectively. TiO₂(A) (99.8% purity) and TiO₂(R) (99.8% purity) were purchased from Aladdin industrial corporation. P25 contains both anatase and rutile phase and was purchased from Degussa Co.

The Co₃O₄/TiO₂ catalysts were prepared by a deposition-precipitation (DP) method. Weighed Co(NO₃)₂·6H₂O were dissolved in 100 ml de-ionized water at room temperature, and then 3 g TiO₂ (less than 100 mesh) fully dispersed in the above solution. The sodium carbonate solution (1 M) was added to this suspension under continuous stirring until pH reached 10. This suspension was aged under stirring for 30 min and statically for 2 h, and then the precipitates were filtered, washed with de-ionized water several times, dried in air at 80 °C and calcined at 350 °C for 3 h in a muffle furnace. The synthesized catalysts are denoted as Co₃O₄/TiO₂(A), Co₃O₄/TiO₂(P25) and Co₃O₄/TiO₂(R) according to the crystalline phase of the TiO₂ support. The metal oxide loading was 10 wt.% on the support.

2.2. Catalytic activity testing

The activities of catalysts for CO oxidation were tested in a continuous flow quartz tube micro-reactor (Φ 8 mm × 23 cm). 200 mg catalyst (40–60 mesh) was packed in the middle of the reactor. The flow rate of feed gas consisted of 1 % CO, 10 % O₂ and 89 % N₂ was 20 ml/min. Before activity testing, the catalyst was pretreated in N₂ flow at 450 °C for 30 min and then cooled down to room temperature.

2.3. Characterization of catalysts

The BET surface areas of samples were measured by N₂ adsorption/desorption at –196 °C on a micromeritics ASAP-2020 instrument, and calculated by the Brunauer–Emmett–Teller (BET) method. Powder X-ray diffraction (XRD) patterns were recorded on a PANalytical PW 3040/60 X'Pert Pro powder diffractometer with CuKα radiation, which was operated at 40 kV and 40 mA and a scanning speed was 0.5 °/min. High resolution transmission electron microscopy (HR-TEM) images were obtained on a JEOL JEM-2100 microscope operated at 200 kV, and the sample to be measured was first dispersed in ethanol and then collected on a copper grids covered with carbon film. After the liquid phase was evaporated the grid was loaded into the microscope. The EPR spectra were obtained on a Bruker EMX-8/2.7 EPR Spectrometer. Laser Raman spectra of samples were obtained on a Renishaw Raman spectrometer at ambient condition and the 514 nm line of a Spectra Physics Ar⁺ laser was used as an excitation. The laser beam intensity and the spectrum slit width were 2 mW and 3.5 cm⁻¹, respectively. X-ray photoelectron spectroscopy (XPS) spectra of samples were obtained on a Kratos Axis Ultra-DLD photoelectron spectrometer equipped with AlKα (1486.6 eV) radiation as the excitation source. All binding energies (BE) were determined with respect to the C1s line (284.8 eV) originating from adventitious carbon.

H₂-Temperature programmed reduction (H₂-TPR) was performed in a quartz U-tube with 50 mg sample. After the sample was pretreated in N₂ at 450 °C for 30 min, it was cooled down to room temperature, and then the reduction gas of 10 vol.% H₂/N₂ (25 ml/min) was used instead of N₂. The heating rate

was 10 °C/min. The uptake amounts of H₂ were measured by a thermal conductivity detector (TCD).

3. Results and Discussion

3.1. Catalytic activity

The catalytic conversions of CO as a function of the reaction temperature over three catalysts under dry or moist conditions are shown in Fig. 1. The results show that three catalysts exhibit pretty good activity for CO oxidation under dry condition, and CO can be oxidized to CO₂ at ambient temperature. Among the three catalysts, Co₃O₄/TiO₂(A) shows the best activity for CO oxidation, in which the reaction temperature of the CO complete conversion (T_{100}) is –43 °C. For the Co₃O₄/TiO₂(P25) and Co₃O₄/TiO₂(R) catalysts, their T_{100} are increased to –2 °C and 45 °C respectively. Under moist condition (0.1 % H₂O), the activities of three catalysts are decreased, their T_{50} (the reaction temperature for 50% CO conversion) are raised by 6–8 °C. The reason is that water might occupy the active sites of cobalt oxide, resulting in a deactivation of the catalyst.

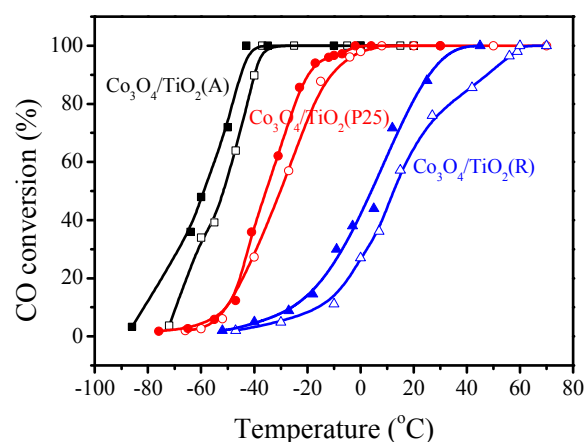


Figure 1. The catalytic activities of Co₃O₄/TiO₂ catalyst (200 mg) for CO oxidation under dry condition (solid symbol) and 0.1 % H₂O condition (hollow symbol).

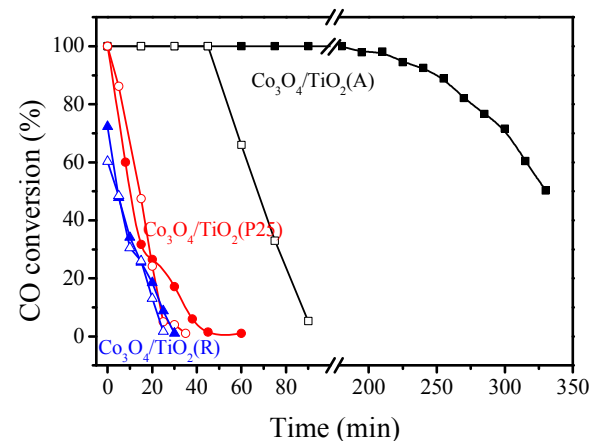


Figure 2. The long-term stabilities of Co₃O₄/TiO₂ catalysts for CO oxidation under dry condition (solid symbol) and 0.1 % H₂O condition (hollow symbol) at 15 °C.

The stabilities of the catalysts under dry or moist condition were also tested at 15 °C. As the results in Fig. 2 show, the

stability of $\text{Co}_3\text{O}_4/\text{TiO}_2(\text{A})$ is the best among three catalysts, its CO conversion can be maintained at 100 % after 180 min of reaction under dry condition, and then its activity is decreased. Under moist condition, because of the poison effect of water, the activity of $\text{Co}_3\text{O}_4/\text{TiO}_2(\text{A})$ is decreased much faster than that under dry condition. As for $\text{Co}_3\text{O}_4/\text{TiO}_2(\text{P25})$ and $\text{Co}_3\text{O}_4/\text{TiO}_2(\text{R})$, their activities are decreased since the reaction begins, and totally lost after 60 min of reaction, no matter under dry or moist condition.

Even so, the results above (Figures 1 and 2) indicate that the crystalline phase of TiO_2 support has an obvious influence on the performance of $\text{Co}_3\text{O}_4/\text{TiO}_2$ catalyst for CO oxidation. As $\text{Co}_3\text{O}_4/\text{TiO}_2(\text{R})$ deactivates more early than other two samples, its light-off curve shows the shallower slope than that of other two samples, because a deactivation of the active sites on $\text{Co}_3\text{O}_4/\text{TiO}_2(\text{R})$ have taken place ceaselessly when the reaction temperature rose.

3.2. N_2 adsorption-desorption and XRD

With the help of low-temperature N_2 adsorption, the BET surface areas (S_{BET}) of $\text{Co}_3\text{O}_4/\text{TiO}_2(\text{A})$, $\text{Co}_3\text{O}_4/\text{TiO}_2(\text{P25})$ and $\text{Co}_3\text{O}_4/\text{TiO}_2(\text{R})$ were measured, and 91.8 m^2/g , 48.7 m^2/g and 38.0 m^2/g , respectively. These results illustrate that Co_3O_4 supported on anatase TiO_2 owns a larger BET surface area than other two catalysts, which may be one of the reasons for its high catalytic activity for CO oxidation.

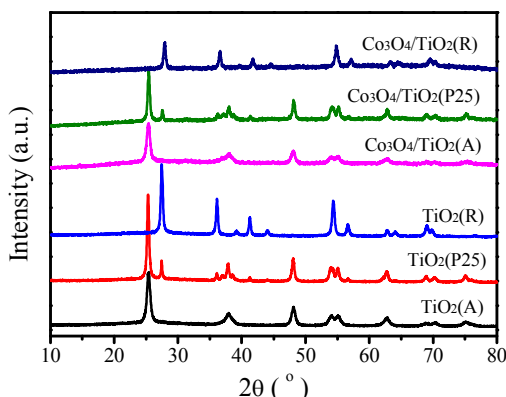


Figure 3. XRD patterns of the $\text{Co}_3\text{O}_4/\text{TiO}_2$ catalysts and the TiO_2 supports.

Table 1. The BET surface area (S_{BET}), crystal size and T_{100} values of the catalysts.

Catalyst	S_{BET} (m^2/g)	Crystal size (nm)	T_{100} ($^{\circ}\text{C}$)
$\text{Co}_3\text{O}_4/\text{TiO}_2(\text{A})$	91.8	15.60	-43
$\text{Co}_3\text{O}_4/\text{TiO}_2(\text{P25})$	48.7	20.02(A), 20.39(R)	-2
$\text{Co}_3\text{O}_4/\text{TiO}_2(\text{R})$	38.0	22.88	45

The XRD patterns of three TiO_2 supports and three $\text{Co}_3\text{O}_4/\text{TiO}_2$ catalysts are shown in Fig. 3. The characteristic diffraction peaks of anatase TiO_2 were detected at $2\theta = 25.4^{\circ}$ (101), 37.9° (004) and 48.1° (200), and the diffraction peaks of rutile TiO_2 are located at $2\theta = 27.5^{\circ}$ (110), 36.1° (101) and 54.4° (211). The crystallite sizes of the supports were calculated by Sherrer's equation²⁸ and shown in Table 1. The results show that the crystallite size of $\text{TiO}_2(\text{R}) > \text{TiO}_2(\text{P25}) > \text{TiO}_2(\text{A})$. In the XRD patterns of Co_3O_4 supported on different supports, the

characteristic XRD peaks of Co_3O_4 cannot be observed, indicating that Co_3O_4 particles highly dispersed on the support or its particles are too small to be detected by XRD.

3.3. High-resolution Transmission Electron Microscopy (HR-TEM)

Representative HR-TEM images of $\text{Co}_3\text{O}_4/\text{TiO}_2(\text{A})$, $\text{Co}_3\text{O}_4/\text{TiO}_2(\text{P25})$ and $\text{Co}_3\text{O}_4/\text{TiO}_2(\text{R})$ catalysts are shown in Fig. 4. The crystallite sizes of three catalysts are 10–30 nm and the rank of the crystallite size is $\text{Co}_3\text{O}_4/\text{TiO}_2(\text{A}) > \text{Co}_3\text{O}_4/\text{TiO}_2(\text{P25}) > \text{Co}_3\text{O}_4/\text{TiO}_2(\text{R})$, which is in agreement with the calculated results by Scherrer formula on the basis of the X-ray diffraction peak broadening. It is difficult to distinguish Co_3O_4 from TiO_2 in the TEM images. In the HR-TEM image (Fig. 4B), Co_3O_4 crystallites can be observed by the help of the ordered fingerprints with the space distance (0.243 nm) between (311) facets in the crystalline Co_3O_4 (in white rectangle). The TiO_2 crystallites which were shown in white circle can be distinguished by the space distance (0.352 nm) between (101) facets in the crystalline anatase TiO_2 .

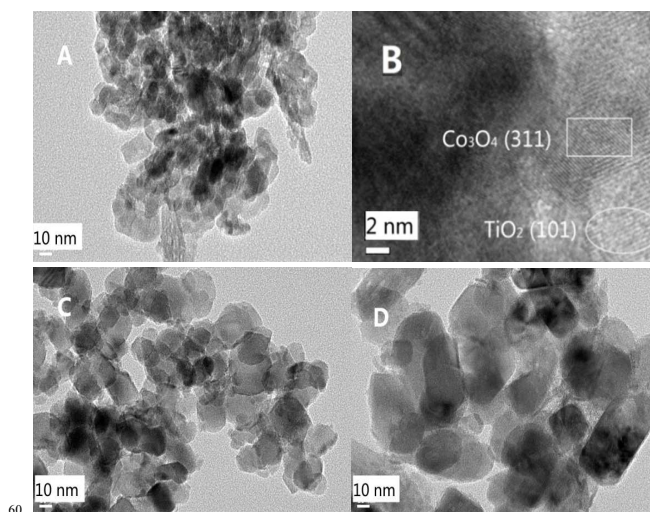


Figure 4. HR-TEM images of (A and B) $\text{Co}_3\text{O}_4/\text{TiO}_2(\text{A})$, (C) $\text{Co}_3\text{O}_4/\text{TiO}_2(\text{P25})$ and (D) $\text{Co}_3\text{O}_4/\text{TiO}_2(\text{R})$ catalysts.

3.4. Electron Paramagnetic Resonance (EPR)

EPR is a useful technique for obtaining information on the electronic structure of solid catalysts. The EPR spectra of $\text{Co}_3\text{O}_4/\text{TiO}_2$ catalysts are shown in Fig. 5A, and that of TiO_2 supports are shown in Fig. 5B. The signals of g values less than 2 were assigned to Ti^{3+} ($3d^1$)^{17,29,30}. Ti^{3+} species are produced by the trapping of electrons at defective sites in TiO_2 ³¹. The signals for $g_{\perp} = 1.996$ and $g_{\parallel} = 1.966$ can be attributed to electrons trapped in Ti^{3+} sites^{25,32}. As can be observed, the EPR signal of Ti^{3+} can be found on $\text{Co}_3\text{O}_4/\text{TiO}_2(\text{A})$ and $\text{TiO}_2(\text{A})$ support, and their EPR spectra are almost the same, indicating that Ti^{3+} exists in $\text{TiO}_2(\text{A})$ and after Co_3O_4 loading it still maintains. Comparing with $\text{Co}_3\text{O}_4/\text{TiO}_2(\text{A})$, and the Ti^{3+} signals on $\text{Co}_3\text{O}_4/\text{TiO}_2(\text{P25})$ and $\text{Co}_3\text{O}_4/\text{TiO}_2(\text{R})$ are weakened and broadened, which are contributed to the formation of diamagnetically coupled Ti^{3+} pairs or the coupling of no-diamagnetic Ti^{3+} ions.³³ For $\text{TiO}_2(\text{R})$, its EPR signal is obviously increased after Co_3O_4 loading, and Ti^{3+} ions in $\text{Co}_3\text{O}_4/\text{TiO}_2(\text{R})$ tend to coupling. As for $\text{TiO}_2(\text{P25})$ or $\text{Co}_3\text{O}_4/\text{TiO}_2(\text{P25})$, both the EPR signals are very weak and broad,

attributing to the structure complexity of the catalyst or a mixture of anatase and rutile TiO₂.

It was reported that, the *g* values in the EPR spectra of TiO₂ are usually below 2.1^{29–34}, and a resonance at *g*=1.979 is characteristic of electrons trapped in tetrahedral Ti⁴⁺ sites in rutile TiO₂³⁴. In the EPR spectrum of Co₃O₄/TiO₂(R), the signal at *g* = 2.019 is probably caused by the interaction between Co₃O₄ and TiO₂(R), and the resonance at *g*=2.278 is caused by the widening of the peak, relating to the relaxation time of spin transition. The formation of Ti³⁺ ions can be assumed to represent an unstable state, which can have a significant influence on the crystalline and interfacial region of TiO₂ between deposited Co₃O₄ and TiO₂ support. The strong signal of Ti³⁺ in Co₃O₄/TiO₂(A) indicates that the catalyst contains defective structure, which promotes the catalytic performance of Co₃O₄/TiO₂(A) for CO oxidation.

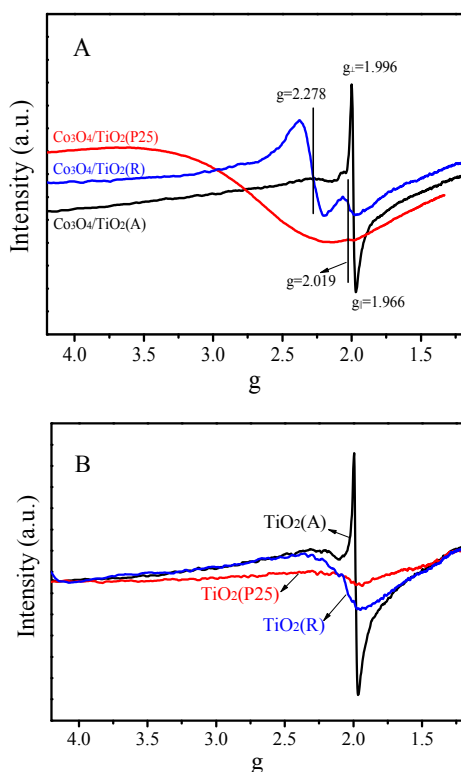


Figure 5. EPR spectra of the Co₃O₄/TiO₂ catalysts (A) and the TiO₂ supports (B).

3.5. Laser Raman Spectroscopy

Fig. 6 shows the laser Raman spectra of the TiO₂ supports and Co₃O₄/TiO₂ catalysts. The results show that the vibration bands of anatase TiO₂ are located at 142, 197, 396, 516, and 639 cm⁻¹^{35–37}, and the vibration bands of rutile TiO₂ are located at 236, 447, and 610 cm⁻¹^{38,39}. In the Raman spectrum of TiO₂(P25), there are the vibration bands of anatase and rutile TiO₂. After Co₃O₄ loading, the Raman vibration bands of TiO₂ are broadened, which may be attributed to an interaction of TiO₂ with cobalt species and disorder in the oxygen sublattice⁴⁰. It was reported that there are some vibration bands at 193, 475, 516, 615, and 680 cm⁻¹ in the Raman spectra of Co₃O₄^{35–37,41}, in which the band around 680 cm⁻¹ is attributed to the A_{1g} symmetry.⁴² The vibration band of A_{1g} on Co₃O₄/TiO₂(A) appeared at 679

cm⁻¹, the lowest wavenumber among three catalysts, which is a sensitive indication for the highly defective structure⁴³. The defective structure is known to play crucial role in the CO oxidation⁴⁴, which may be related to its high catalytic activity. For the Co₃O₄/TiO₂(P25) catalyst, there are two bands of Co₃O₄ at 475 and 682 cm⁻¹.

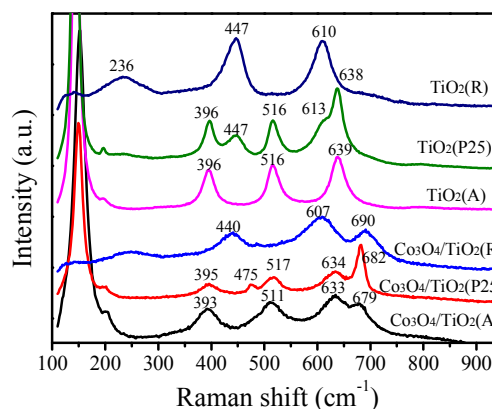


Figure 6. Laser Raman spectra of the synthesized catalysts and supports.

3.6. X-ray photoelectron spectroscopy (XPS)

The surface properties of the supported catalysts were further explored by XPS, and the peak-fitting Co 2p XPS spectra of three catalysts are shown in Fig. 7. It was reported the binding energies of Co³⁺ and Co²⁺ ions are 780.2 ± 0.6 and 781.8 ± 0.6 eV, respectively⁴⁵, and the energy difference between the Co 2p_{3/2} peak and the Co 2p_{1/2} peak is approximately 15 eV. Two small peaks at 786.3 eV and 804.8 eV are the shake-up satellite peaks of Co²⁺. The binding energies of Co 2p_{3/2} and Co 2p_{1/2} of Co₃O₄/TiO₂ catalysts were summarized in Table 2. The results show that the binding energies of Co 2p in the spectra of Co₃O₄/TiO₂(A) and Co₃O₄/TiO₂(P25) are smaller than that of Co₃O₄/TiO₂(R), indicating that the electron binding ability of Co ions in the Co₃O₄/TiO₂(R) catalyst is bigger than that in other two catalysts and the structure nature of TiO₂ support affects the electron transfer ability of Co ions on the TiO₂ support. In addition, we can find, the peak area of Co₃O₄/TiO₂(R) is the highest among three catalysts, which might be caused by the lowest surface area of TiO₂(R). As the Co₃O₄ loading is the same for three catalysts, the smaller surface area makes the concentration of Co relatively higher.

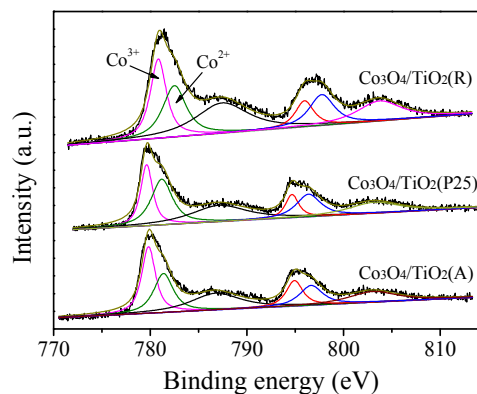


Figure 7. The Co 2p XPS spectra of Co₃O₄/TiO₂ catalysts.

Table 2. XPS data (binding energies of Co 2p_{3/2}, Co 2p_{1/2} and O 1s, O_{ads}/O_{lat} of Co₃O₄/TiO₂(A), Co₃O₄/TiO₂(P25) and Co₃O₄/TiO₂(R).

Catalyst	Co 2p _{3/2} (eV)	Co 2p _{1/2} (eV)	O 1s (eV)	O _{ads} /O _{lat}	Ti 2P _{3/2} (eV)	Ti 2P _{1/2} (eV)
Co ₃ O ₄ /TiO ₂ (A)	779.8	794.9	529.7	0.58	458.6	464.4
	781.4	796.6	530.3			
			531.6			
Co ₃ O ₄ /TiO ₂ (P25)	779.6	794.7	529.9	0.49	458.9	464.7
	781.2	796.4	530.5			
			531.8			
Co ₃ O ₄ /TiO ₂ (R)	780.8	795.9	530.2	0.72	458.9	464.7
	782.5	797.7	531.1			
			532.4			

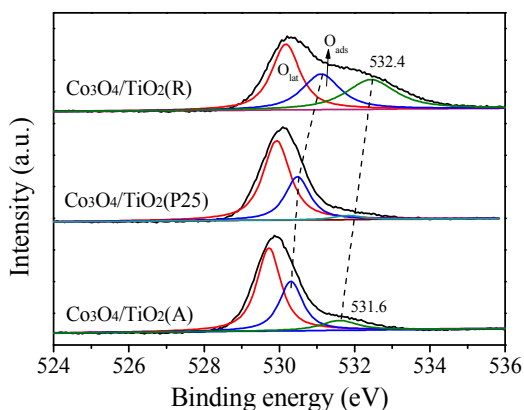
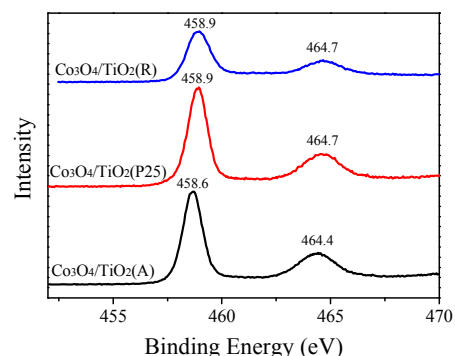
**Figure 8.** The O 1s XPS spectra of Co₃O₄/TiO₂ catalysts.

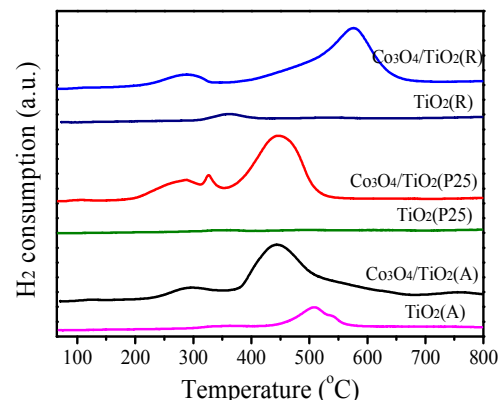
Fig. 8 shows the O 1s XPS spectra of three catalysts. The O 1s peak can be fitted to three kinds of Gaussian peaks. The peak at 529.0–530.2 eV (binding energy) should be assigned to surface lattice oxygen (O_{lat}), the peak at 530.3–531.1 eV can be assigned to adsorbed oxygen (O_{ads}, O⁻, O₂⁻ or O₂²⁻) species, and the peak at 531.6–532.5 eV is commonly ascribed to adsorbed H₂O or surface carbonate^{46–48}. The adsorbed oxygen species of O⁻ and O₂⁻ are known to be active for oxygen exchange and CO oxidation^{49–51}. The results in Fig. 8 show that, the O_{ads} peak gradually shifted to higher binding energy from Co₃O₄/TiO₂(A) to Co₃O₄/TiO₂(R), indicating that the electronic density of oxygen is decreased, which may be attributed to the contribution of surface hydroxyl group bounded to cobalt or titanium ion. The peak of surface hydroxyl and carbonate on Co₃O₄/TiO₂(R) is much stronger than that on other two catalysts, resulting in blocking of the active sites for CO adsorption, which is usually considered as a deactivation reason of the catalysts for CO oxidation^{52,53}. Therefore, the surface of Co₃O₄/TiO₂(R) is easily covered by carbonate and hydroxyl groups, resulting in a decrease in its catalytic activity, which can be further verified by the O 1s peak of surface carbonate at 532.4 eV. The ratios of O_{ads}/O_{lat} in Table 2 show that, Co₃O₄/TiO₂(A) with O_{ads}/O_{lat} = 0.58 exhibits the highest activity, and Co₃O₄/TiO₂(A) with O_{ads}/O_{lat} = 0.72 shows that the lowest activity, which should be ascribed to the presence of carbonates on Co₃O₄/TiO₂(A) to inhibit adsorption of CO on the catalyst surface. The results above show that a relatively clean surface with more adsorbed

oxygen is beneficial to improve the catalytic activity of the Co₃O₄/TiO₂ catalyst for CO oxidation.

In the Ti 2p XPS spectra in Fig. 9, the peaks of Ti 2p_{3/2} and Ti 2p_{1/2} are located at 458.6 and 464.4 eV respectively, which agree well with the values reported.⁵⁴ As can be observed, the peak intensity of Co₃O₄/TiO₂(R) is much lower than other two catalysts, which may be caused by its lower surface area. The Ti 2p peaks of Co₃O₄/TiO₂(P25) and Co₃O₄/TiO₂(R) shifts to higher binding energy than Co₃O₄/TiO₂(A), indicating that Ti ions in Co₃O₄/TiO₂(P25) and Co₃O₄/TiO₂(R) possess higher valence state than that in Co₃O₄/TiO₂(R). The binding energies of Ti 2p are listed in Table 2.

**Figure 9.** The Ti 2p XPS spectra of Co₃O₄/TiO₂ catalysts.

3.7. H₂-TPR

**Figure 10.** H₂-TPR profiles of the Co₃O₄/TiO₂ catalysts and TiO₂ supports.

The H₂-TPR profiles of the Co₃O₄/TiO₂ catalysts and TiO₂ supports are shown in Fig. 10. The results show that the TiO₂ supports exhibit the pretty weak reduction peaks, so that the reduction peaks of the Co₃O₄/TiO₂ catalysts are mainly results from the reduction of Co₃O₄. Co₃O₄/TiO₂(A) exhibit two reduction peaks at ~297 °C and 445 °C. The peak at 200–350 °C may be attributed to the reduction of Co³⁺ to Co²⁺, and the peak at 350–700 °C can be attributed to the reduction of Co²⁺ to Co⁰.^{55,56} For the Co₃O₄/TiO₂(P25) catalyst, its TPR reduction peaks are similar to that of the Co₃O₄/TiO₂(A) catalyst, except the small peak at 325 °C. However, the reason of the reduction peak formation at 325 °C is unclear, and it may be the reduction of Co³⁺ on the interfacial region between anatase and rutile TiO₂. Unlike the TPR curves of Co₃O₄/TiO₂(A) and Co₃O₄/TiO₂(P25), the high-temperature reduction peak of Co₃O₄/TiO₂(R) shifts

~575 °C. Thus Co^{2+} on anatase TiO_2 is easily reduced compared with Co^{2+} on rutile TiO_2 . That is to say, the reducibility of Co_3O_4 (special for Co^{2+}) is obviously affected by the structure of TiO_2 support. Anatase TiO_2 supported Co_3O_4 catalysts shows the best reducibility, which results probably in its high catalytic performance for CO oxidation.

3.8. Discussion

For the supported catalysts, the supports often play a crucial role in the performance of catalysts with the help of an interaction between active components and support. TiO_2 has three main crystalline structures: anatase (tetragonal $I4/amd$), brookite (orthorhombic $Pcab$), and rutile (tetragonal $P42/mnm$), and anatase and rutile are usually used as catalyst supports, among them, anatase tends to be more stable at low temperature and rutile is the stable form at higher temperature. And the reactivity of anatase is higher than rutile. Nanba *et al.*²⁶ found that TiO_2 crystal phase could affect the oxidation state of Ag supported on TiO_2 catalyst for acrylonitrile decomposition, that is Ag particles on anatase TiO_2 was of an oxidized state and that on rutile was metallic. Kang *et al.*⁵⁷ investigated CO oxidation over CuO/TiO_2 , and found that CuO dispersion, an interaction between CuO and TiO_2 and the oxidation state of copper component were changed by the crystal structure of TiO_2 support, and the catalytic activity of the catalyst supported on rutile TiO_2 was the highest. For different reactions with different catalysts, the effect of the crystal phase of TiO_2 on the catalytic performance might not be the same. Herein, the CO oxidation over $\text{Co}_3\text{O}_4/\text{TiO}_2$ was investigated, and the effect of the crystal phase of TiO_2 on the catalytic performance of Co_3O_4 catalyst was discussed.

The $\text{Co}_3\text{O}_4/\text{TiO}_2(\text{A})$ catalyst exhibits the higher activity and better stability for CO oxidation than $\text{Co}_3\text{O}_4/\text{TiO}_2(\text{P25})$ and $\text{Co}_3\text{O}_4/\text{TiO}_2(\text{R})$ (Figs. 1 and 2), which may be attributed to the following reasons. (1) The $\text{Co}_3\text{O}_4/\text{TiO}_2(\text{A})$ catalyst owns a higher BET surface area and smaller crystalline size than other two catalysts. As the diffraction peaks of Co_3O_4 cannot be detected in the XRD profiles (Fig. 3), Co_3O_4 is highly dispersed on TiO_2 support and close interacted with the support. (2) The EPR results (Fig. 5) indicate that Ti^{3+} species only exists in $\text{Co}_3\text{O}_4/\text{TiO}_2(\text{A})$, which is of unstable state and has a significant influence on the catalytic property of the catalyst. (3) In the Raman spectra (Fig. 6), the A_{1g} peak of Co_3O_4 shifted to lower wavenumber when anatase TiO_2 was used as the support, which illustrates a highly defective structure of $\text{Co}_3\text{O}_4/\text{TiO}_2(\text{A})$ and plays a crucial role in the CO oxidation. (4) The electron transfer ability of Co ions was enhanced by the help of the anatase TiO_2 support, resulting in a good oxygen adsorption ability of $\text{Co}_3\text{O}_4/\text{TiO}_2(\text{A})$ by means of the clean surface, which were verified by the XPS results (Figs. 7 and 8). (5) The H_2 reduction behaviour of Co_3O_4 is improved due to the presence of anatase TiO_2 support (Fig. 10), unlike $\text{Co}_3\text{O}_4/\text{TiO}_2(\text{R})$ and $\text{Co}_3\text{O}_4/\text{TiO}_2(\text{P25})$.

The results above show that the physicochemical properties of Co_3O_4 can be varied by the crystal structure of TiO_2 support. The presence of Ti^{3+} ions in $\text{Co}_3\text{O}_4/\text{TiO}_2(\text{A})$ as a defective structure, is in favour of forming oxygen vacancies⁵⁸, which was observed in Raman spectra (Fig. 6). The oxygen vacancies can adsorb oxygen from gas phase and weaken its bond to form the activated oxygen species⁵⁹. The activated oxygen species could accelerate the oxygen exchange and surface diffusion to promote the catalytic

oxidation of CO. In other words, the defective structure can accelerate the oxygen exchange and surface diffusion to prevent the formation of carbonate species and slow down the accumulation of carbonate species, resulting in an increase in the catalytic activity for CO oxidation, which was verified by the O1s XPS spectra (Fig. 8), because the accumulation of carbonate species on the surface would lead to the decrease of the catalytic activity for CO oxidation^{52,53}.

Furthermore, the reducibility of Co_3O_4 is also affected by the crystalline structure of the TiO_2 support, and the reduction temperature of $\text{Co}_3\text{O}_4/\text{TiO}_2(\text{A})$ is lower compared with the other two catalysts. In the process of CO oxidation, the reduction of Co ions is a very important step in the redox catalytic cycle, which plays a crucial role in the CO oxidation.

4. Conclusions

Highly dispersed Co_3O_4 nanoparticles supported on three sorts of TiO_2 with different crystalline structures (anatase phase TiO_2 (A), P25 (Degussa) and rutile phase TiO_2 (R)) were prepared by a deposition-precipitation method. The results show that the crystalline structure of TiO_2 would affect obviously the physicochemical and catalytic properties of the $\text{Co}_3\text{O}_4/\text{TiO}_2$ catalysts, and the $\text{Co}_3\text{O}_4/\text{TiO}_2(\text{A})$ catalyst exhibits the highest activity for CO oxidation among three $\text{Co}_3\text{O}_4/\text{TiO}_2$ catalysts. The excellent catalytic performance of the $\text{Co}_3\text{O}_4/\text{TiO}_2(\text{A})$ catalyst for CO oxidation can be attributed to the following reasons:

(1) The $\text{Co}_3\text{O}_4/\text{TiO}_2(\text{A})$ catalyst owns a higher BET surface area and smaller crystalline size than $\text{Co}_3\text{O}_4/\text{TiO}_2(\text{P25})$ and $\text{Co}_3\text{O}_4/\text{TiO}_2(\text{R})$. And Co_3O_4 is highly dispersed on TiO_2 support and close interacted with the support.

(2) The Ti^{3+} species exists in $\text{Co}_3\text{O}_4/\text{TiO}_2(\text{A})$, which is of unstable state and has a significant influence on the catalytic property of the catalyst. And $\text{Co}_3\text{O}_4/\text{TiO}_2(\text{A})$ exhibits a highly defective structure that plays a crucial role in the CO oxidation.

(3) The electron transfer ability of Co ions was enhanced by the help of the anatase TiO_2 support, resulting in a good oxygen adsorption ability of $\text{Co}_3\text{O}_4/\text{TiO}_2(\text{A})$ by means of the clean surface. The reducibility of Co_3O_4 is improved due to the presence of anatase TiO_2 support, so that $\text{Co}_3\text{O}_4/\text{TiO}_2(\text{A})$ possesses the best redox property among three $\text{Co}_3\text{O}_4/\text{TiO}_2$ catalysts.

Acknowledgements

This project was financially supported by National Natural Science Foundation of China (21273150), the National Basic Research Program of China (2010CB732300, 2013CB933201), the national high technology research and development program of China (2011AA03A406, 2012AA062703), the Fundamental Research Funds for the Central Universities, the ‘‘ShuGuang’’ Project (10GG23) of Shanghai Municipal Education Commission.

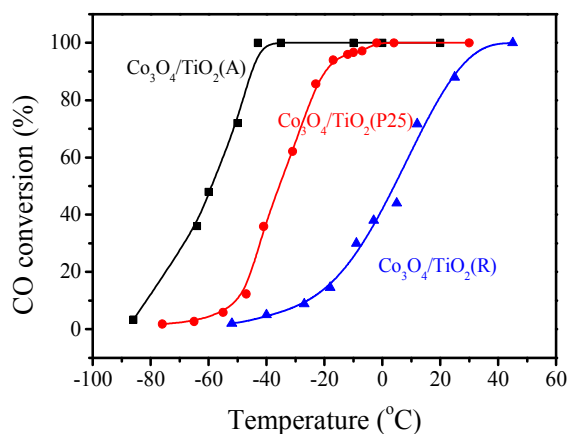
Notes and references

^a Key Laboratory for Advanced Materials and Research Institute of Industrial catalysis, East China University of Science and Technology, Shanghai 200237, P. R. China. Fax: +86-21-64253824 E-mail: gzhlu@ecust.edu.cn (G.Z. LU).

- ^b Research Institute of Applied Catalysis, Shanghai Institute of Technology, Shanghai 200235, P. R. China.
- 1 M. Shelef and R.W. McCabe, *Catal. Tod.*, 2000, **62**, 35.
 - 2 M.V. Twigg, *Appl. Catal. B*, 2007, **70**, 2.
 - 3 Y.X. Shen, G.Z. Lu, Y. Guo and Y.Q. Wang, *Chem. Commun.*, 2010, **46**, 8433.
 - 4 A. Saramat, P. Thormählen, M. Skoglundha, G. S. Attard and A.E.C. Palmqvist, *J. Catal.*, 2008, **253**, 253.
 - 5 N. Lopez, T.V.W. Janssens, B.S. Clausen, Y. Xu, M. Mavrikakis, T. Bligaard and J.K. Nørskov, *J. Catal.*, 2004, **223**, 232.
 - 6 M. Haruta, T. Kobayashi, H. Sano and N. Yamada, *Chem. Lett.*, 1987, **16**, 405.
 - 7 J. Jansson, *J. Catal.*, 2000, **194**, 55.
 - 8 J. Jansson, A.E.C. Palmqvist, E. Fridell, M. Skoglundh, L.O. Sterlund, P. Thormählen and V. Langer, *J. Catal.*, 2002, **211**, 387.
 - 9 H.K. Lin, C.B. Wang, H.C. Chiu and S.H. Chien, *Catal. Lett.*, 2003, **86**, 63.
 - 10 H.K. Lin, H.C. Chiu, H.C. Tsai, S.H. Chien and C.B. Wang, *Catal. Lett.*, 2003, **88**, 169.
 - 11 D.A.H. Cunningham, T. Kobayashi, N. Kamijo and M. Haruta, *Catal. Lett.*, 1994, **25**, 257.
 - 12 P. Thormählen, M. Skoglundh, E. Fridell and B. Andersson, *J. Catal.*, 1999, **188**, 300.
 - 13 Y.Z. Wang, Y.X. Zhao, C.G. Gao, D.S. Liu, *Catal. Lett.*, 2007, **116**, 136.
 - 14 X.W. Xie, Y. Li, Z.Q. Liu, M. Haruta and W.J. Shen, *Nature*, 2009, **458**, 746.
 - 15 J. Li, G.Z. Lu, G.S. Wu, D.S. Mao, Y.Q. Wang and Y. Guo, *Catal. Sci. Technol.*, 2012, **2**, 1865.
 - 16 J. Li, G.Z. Lu, G.S. Wu, D.S. Mao, Y.L. Guo, Y.Q. Wang and Y. Guo, *RSC Adv.*, 2013, **3**, 12409.
 - 17 J. Panpranot, K. Kontapakdee and P. Praserthdam, *J. Phys. Chem. B.*, 2006, **110**, 8019.
 - 18 P. Weerachawanasak, O. Mekasuwandumrong, M. Arai, S.I. Fujita, P. Praserthdam and J. Panpranot, *J. Catal.*, 2009, **262**, 199.
 - 19 P. Castillo-Villalón and J. Ramírez, *J. Catal.*, 2009, **268**, 39.
 - 20 F. Cárdenas-Lizana, S. Gómez-Quero, H. Idriss and M.A. Keane, *J. Catal.*, 2009, **268**, 223.
 - 21 C.H. Lin, J.H. Chao, C.H. Liu, J.C. Chang and F.C. Wang, *Langmuir*, 2008, **24**, 9907.
 - 22 G. Li, N.M. Dimitrijevic, L. Chen, T. Rajh and K.A. Gray, *J. Phys. Chem. C*, 2008, **112**, 19040.
 - 23 L.G. Devi, N. Kottam and S.G. Kumar, *J. Phys. Chem. C*, 2009, **113**, 15593.
 - 24 B. Ohtani, O.O.P. Mahaney, F. Amano, N. Murakami and R. Abe, *J. Adv. Oxid. Technol.*, 2010, **13**, 247.
 - 25 Y. Li, B. Xu, Y. Fan, N. Feng, A. Qiu, J.W. Miao, J. He, H. Yang and Y. Chen, *J. Mol. Catal. A Chem.*, 2004, **216**, 107.
 - 26 T. Nanba, S. Masukawa, J. Uchisawa and A. Obuchi, *Appl. Catal. A*, 2012, **419-420**, 49.
 - 27 H. Iida and A. Igarashi, *Appl. Catal. A*, 2006, **298**, 152.
 - 28 A. Patterson, *Phys. Rev.*, 1939, **56**, 978.
 - 29 J.C. Conesa, P. Malet, G.M. Unuera, J. Sanz and J. Soria, *J. Phys. Chem.*, 1984, **88**, 2986.
 - 30 T.M. Salama, H. Hattori, H. Kita, K. Ebitani and T. Tanaka, *J. ChemSoc. Faraday Trans.*, 1993, **89**, 2067.
 - 31 S. Ikeda, N. Sugiyama, S.Y. Murakami, H. Kominami, Y. Kera, H. Noguchi, K. Uosaki, T. Torimoto and B. Ohtani, *Phys. Chem. Chem. Phys.*, 2003, **5**, 778.
 - 32 L. Bonnevot and G.L. Haller, *J. Catal.*, 1988, **113**, 96.
 - 33 P. Claus, S. Schimpt, R. Schodel, P. Kraak, W. Morke and D. Honicke, *Appl. Catal. A*, 1997, **165**, 429.
 - 34 G.H. Li, N.M. Dimitrijevic, L. Chen, J.M. Nichols, T. Rajh and K.A. Gray, *J. Am. Chem. Soc.*, 2008, **130**, 5402.
 - 35 T. Xiao, S.J. Ji, H. Wang, K.S. Coleman and M.L.H. Green, *J. Mol. Catal. A.*, 2001, **175**, 111.
 - 36 Y. Brik, M. Kacimi, M. Ziyad and F. Bozon-Verduraz, *J. Catal.*, 2001, **202**, 118.
 - 37 Y. Brik, M. Kacimi, F. Bozon-Verduraz and M. Ziyad, *J. Catal.*, 2002, **211**, 470.
 - 38 M.S. Wainwright and N.R. Foster, *Catal. Ver.*, 1979, **19**, 211.
 - 39 M. Wu, W. Zhang, Z. Du and Y. Huang, *Mod. Phys. Lett. B*, 1999, **13**, 167.
 - 40 J. Cai, C. Raptis, Y.S. Raptis and E. Anastassakis, *Phys. Rev. B*, 1995, **51**, 201.
 - 41 H. Ohtsuka, T. Tabata, O. Okada, L.M.F. Sabatino and G. Bellussi, *Catal. Lett.*, 1997, **44**, 265.
 - 42 J. Jiang and L.C. Li, *Mater. Lett.*, 2007, **61**, 4894.
 - 43 Q. Liu, L.C. Wang, M. Chen, Y. Cao, H.Y. He and K.N. Fan, *J. Catal.*, 2009, **263**, 104.
 - 44 H.Y. Li, H.F. Wang, Y.L. Guo, G.Z. Lu and P. Hu, *Chem. Comm.*, 2011, **47**, 6105.
 - 45 M. Kang, M.W. Song and C.H. Lee, *Appl. Catal. A*, 2003, **251**, 143.
 - 46 A.F. Carley, M.W. Roberts and A.K. Santra, *J. Phys. Chem. B*, 1997, **101**, 9978.
 - 47 N. Yamazoe, Y. Teraoka and T. Seiyama, *Chem. Lett.*, 1981, 1767.
 - 48 J.L.G. Fierro and L.G. Tejuca, *Appl. Surf. Sci.*, 1987, **27**, 453.
 - 49 C. Naccache, P. Meriaudeau and M. Che, *Trans. Faraday Soc.*, 1971, **67**, 506.
 - 50 V.A. Shvets and V.B. Kazansky, *J. Catal.*, 1972, **25**, 123.
 - 51 M. Che and A.J. Tench, *Adv. Catal.*, 1983, **32**, 1.
 - 52 Y. Denkwitz, A. Karpenko, V. Plzak, R. Leppelt, B. Schumacher and R.J. Behm, *J. Catal.*, 2007, **246**, 74.
 - 53 J. Jansson, M. Skoglundh, E. Fridell and P. Thormählen, *Top. Catal.*, 2001, **16/17**, 385.
 - 54 B.M. Reddy, B. Chowdhury, I. Ganesh, E.P. Reddy, T.C. Rojas and A. Fernandez, *J. Phys. Chem. B*, 1998, **102**, 10176.
 - 55 Y.Y. Liu, T. Hanaoka, T. Miyazawa, K. Murata, K. Okabe and K. Sakanishi, *Fuel. Process. Technol.*, 2009, **90**, 901.
 - 56 D. Shanke, S. Vada, E.A. Blekkan, A.M. Hilmen, A. Hoff and A. Holmen, *J. Catal.*, 1995, **156**, 85.
 - 57 M.Y. Kang, H.J. Yun, S.J. Yu, W. Kim, N.D. Kim and J. Yi, *J. Mol. Catal. A*, 2013, **368-369**, 72.
 - 58 K. Suriye, P. Praserthdam and B. Jongsomjit, *Appl. Surf. Sci.*, 2007, **253**, 3849.
 - 59 Z.P. Hao, D.Y. Cheng, Y. Guo and Y.H. Liang, *Appl. Catal. B*, 2001, **33**, 217.

Effect of TiO₂ crystal structure on the catalytic performance of Co₃O₄/TiO₂ catalyst for low-temperature CO oxidation

Jie Li, Guanzhong Lu,* Guisheng Wu, Dongsen Mao, Yanglong Guo, Yanqin Wang and Yun Guo



The Co₃O₄ supported on TiO₂ (anatase (A), rutile (R) and P25 (Degussa)) catalysts were prepared by a deposition-precipitation method. Co₃O₄/TiO₂(A) shows very excellent activity for CO oxidation with 100% conversion at -43 °C, which is attributed to its highly defective structure, high oxygen adsorption ability and redox property.